


## Article

# A Fluorescent Perspective on Water Structuring: ACDAN in Salt Solutions and Hydrogels

Giuseppe De Luca <sup>†</sup> , Vittorio Ferrara <sup>†</sup>, Bruno Pignataro, Valeria Vetri  and Giuseppe Sancataldo <sup>\*</sup>

Department of Physics and Chemistry-Emilio Segrè, University of Palermo, Viale delle Scienze, Ed.18, 90123 Palermo, Italy

<sup>\*</sup> Correspondence: giuseppe.sancataldo@unipa.it<sup>†</sup> These authors contributed equally to this work.

**Abstract:** The interactions and structural organization of water molecules play a crucial role in a wide range of physical, chemical, and biological processes. The ability of water to form hydrogen bonds (H-bonds) underpins its unique properties and enables it to respond dynamically to various environmental factors. These interactions at the molecular level may affect vital processes like protein folding, enzyme activity, and cellular organization. The presence of solutes and spatial constraints can alter the H-bonding network of water, and these effects are ubiquitous in the biological environment. In this study, we analyzed the fluorescence of 2-acetyl-6-(dimethylamino)naphthalene (ACDAN) fluorescence emission in water solutions containing kosmotropic and chaotropic salts and in agar hydrogels. Recently, this dye has proven invaluable in studying water network structure and dynamics, as its fluorescence signal changes based on the local dielectric environment, revealing variations in the dipolar relaxation of water. Our results show that ACDAN spectral response correlates with the degree of water ordering, providing important insights into solute–water interactions and water dynamics in free and confined environments.

**Keywords:** ACDAN; water network; Hofmeister series; fluorescence; DAN; agar hydrogel; gelification



**Citation:** De Luca, G.; Ferrara, V.; Pignataro, B.; Vetri, V.; Sancataldo, G. A Fluorescent Perspective on Water Structuring: ACDAN in Salt Solutions and Hydrogels. *Biophysica* **2024**, *4*, 619–633. <https://doi.org/10.3390/biophysica4040041>

Academic Editor: Herbert Schneckenburger

Received: 30 October 2024

Revised: 21 November 2024

Accepted: 24 November 2024

Published: 28 November 2024



**Copyright:** © 2024 by the authors. Licensee MDPI, Basel, Switzerland. This article is an open access article distributed under the terms and conditions of the Creative Commons Attribution (CC BY) license (<https://creativecommons.org/licenses/by/4.0/>).

## 1. Introduction

The molecular interactions and structural organization of water are fundamental for numerous physical, chemical, and biological processes [1–5]. Indeed, water plays a key role in all biological processes, actively influencing the stability, dynamics, and function of biomolecules [1]. Beyond being a solvent, water drives, for example, fascinating processes such as liquid–liquid phase separation by modulating hydration entropy and enthalpy and affecting the assembly of biomolecule-rich and dilute phases [2]. In living cells, these water-mediated interactions and the water ability to affect biomolecule behavior are essential for phase separation and the coordination of the biochemical processes involved, for instance in the formation of membranellar organelles, guided by hydrogen bonding, dipole interactions, and changes in water structure [3,5]. This dynamic and versatile behavior of water molecules is mainly related to the formation in the liquid phase of an intricate and dynamic hydrogen bond network. Such an ability of water molecules to form a supramolecular structure hydrogen bond (H-bonds) network is at the basis of its peculiar physical properties, such as surface tension, anomalous density behavior, and high specific heat [6,7]. In addition, the H-bond network modulates biochemical processes, which are of central relevance for the understanding of biomolecular organization and function in life sciences and related technological applications [4,8]. At the molecular scale, H-bonding results in the formation of a dynamic network that is highly sensitive to its molecular surroundings, continuously fluctuating and reorganizing in response to factors such as temperature, solutes, and the proximity to biomolecules. Many examples

on how the presence of solutes may alter the water H-bonding network through solvation and coordination processes in a different way have been reported, as extensively shown for biomolecules [9], with a special focus on proteins which are affected by water in the biochemistry and folding/unfolding [1,10,11], as well as in their supramolecular aggregation [12–14]. The effects of solutes in the water network have been widely investigated by means of different spectroscopic approaches; for example, the use of terahertz and infrared spectroscopy has been applied to probe water networks in the proximity of proteins [15], as well as the use of infrared spectroscopy to investigate changes in the water network due to hydrophilic co-solvents [16], pointing out that the water hydrogen bond network is profoundly influenced by solutes.

Solution conditions such as temperature and the presence of organic or inorganic solutes strongly impact on water structure as well [17–20]. In particular, electrolytes act through electric fields, steric factors, and specific ion properties [17]. They represent a relevant case of this phenomenon since simple electrolytes are almost ubiquitous in environmental and biological water samples, determining a strong modification of the position of coordinated water molecules and altering the H-bonding network, as reported for many kinds of cations [21] and anions [22,23], even in confined environments [24]. In this context, ions are typically classified based on the strength of their interaction with water molecules. As the interaction between ions and water molecules becomes stronger, the energy required for the water molecule to move away from its position near the ion increases, and this is reflected in the ability of salt in controlling the solubility of molecules. The most well-known representation of the ions in terms of their ordering/disordering effect in water is represented by the Hofmeister series [25–30]. Ions in the Hofmeister series are typically categorized as kosmotropes or chaotropes, with the former promoting the stability of proteins by enhancing water bonding and the latter disrupting the hydrogen-bonding network of water [25–27]. In addition to a direct physicochemical interaction between ions and water molecules, an alternative way to modulate water H-bond networks can be by confinement [31,32]. As an example, water order and dynamics can be influenced within nanostructured solid porous materials [33], as well as in intricate supramolecular polymeric nets as for the case of hydrogels [34–37]. The dynamic properties and the molecular organization of water molecules in a restricted environment may critically differ from those of pure bulk water, often resulting in altered thermodynamic and kinetic properties of the system in analysis. This can be attributed to the formation of frustrated H-bond networks within pores or at interfaces. Geometric confinement has been shown to alter the structural and dynamic properties of water, in some instances also hindering the formation of crystalline structure or shifting water orientational relaxation time to higher frequencies [32,38]. As shown by several experiments concerning the water molecules in hydrogels matrices [39–42], different states coexist in these systems, such as free, weakly bound, and strongly bound to the hydrogel network, and the distribution of molecules among these states affects the physicochemical properties of hydrogel.

Significant efforts have been made in developing the understanding of the water H-bonding structure due to its relevance in many fields, ranging from basic to applied sciences [1,4,5,43,44]. Several spectroscopic methods have been employed, such as X-ray diffraction, Neutron diffraction, NMR Relaxation, dielectric relaxation, Terahertz Spectroscopy, and Vibrational Spectroscopy [2,32,40,45–53]. Among them, near-infrared (NIR) spectroscopy has been proven to be one of the most effective experimental techniques for the investigation of hydrogen-bonded networks in liquid water. The NIR absorption spectrum of liquid water exhibits a band around 1450 nm, which primarily detects the overtone and combination modes of fundamental molecular vibrations of the O-H bond, providing insights into the hydrogen-bonding network of water [17,54–57]. The absorption band is sensitive to the structural organization of the water network; specifically, variations in the NIR absorption spectra can reveal the supramolecular organization of water [58]. This band shifts toward shorter wavelengths (higher wavenumbers) as temperature increases, serving as a distinctive marker of structural disorder. Specifically, some studies

have measured the NIR band of water at various temperatures, revealing an isosbestic point [57,59], thus suggesting that at least two components are present in liquid water. The components might be assignable to strongly hydrogen-bonded water and weakly hydrogen-bonded (or non-hydrogen-bonded) water, which causes, respectively, the longer-wavelength (lower-frequency) and the shorter-wavelength (higher-frequency) components of the NIR absorption band of water. Similar behavior has been observed in aqueous solutions containing molecules that are able to organize or disrupt the H-bonding network structure of water [56,60]. NIR spectroscopy was also largely used for the analysis of water dynamics within hydrogels in various contexts, ranging from biological to technological applications, such as in renewable energy [61–63]. Unveiling the role of water molecules in hydrogels enables the investigation of some biological processes occurring in gel-like environments, e.g., cytosol, as well as the characterization of the gelification process itself, a high-relevance process in many applicative fields, such as in biomaterial production [64]. Even in the field of innovative energy technology, hydrogels have found interesting applications as a medium for innovative and sustainable dye-sensitized solar cells, with water molecules playing a fundamental role in mediating the charge carriers flows [65,66].

In this work, we present an experimental study on ACDAN (2-acetyl-6-(dimethylamino)naphthalene), a fluorescent dye aimed at eliciting its properties as a powerful tool for readily investigating water structure and dynamics at the molecular level. ACDAN is part of the (dimethylamino)naphthalene (DAN) family, a group of polarity-sensitive fluorescent probes introduced by Gregorio Weber in the late seventies to monitor solvent relaxation phenomena [67] (see ACDAN chemical structure in Figure S1a, reported in SM). These probes exhibit changes in their fluorescence properties based on the local dielectric environment and water dipolar relaxation dynamics. The most known exponents of the DAN dye family are ACDAN, PRODAN, and LAURDAN. These three dyes have a naphthalene moiety modified on the 2,6 ring positions with an electron donor group (the amine) and an electron acceptor group (the carbonyl group), which generate a dipole moment [67–69]. Among the DAN family, ACDAN is the most hydrophilic, while LAURDAN is the most hydrophobic, and PRODAN stands in between the two. For this reason, these three dyes can be used to study different systems and yet provide similar information about the solvent dipolar relaxation that translates into specificity, depending on the system [68–71].

The photo-physics of ACDAN is well known; its fluorescence depends on the dipolar relaxation of the solvent. A simplified Jablonski diagram is shown in Figure S1b, presented in the Supporting Material (SM). Following an absorption process, the molecule transitions from its ground state to an excited state, where its dipole moment increases. Due to this increase, it can interact with surrounding water molecules, which may reorient themselves toward its dipole. If the water is in a disordered phase, allowing the molecules to rotate freely, ACDAN experiences high dipolar relaxation, which lowers the energy of the excited state, causing a red shift in fluorescence. Conversely, if the water is in a more ordered state and the molecules cannot reorient or rotate, the excited state of ACDAN retains its energy, resulting in the emission of a higher energy (blue) photon. This results in a blue shift in fluorescence. ACDAN spectroscopic properties were recently used to measure water dipolar relaxation in the cell cytosol of oscillating yeast cells [71], water dipolar relaxation in zebra fish lenses [72], water dynamics in the lumen of trafficking lysosomes [73], water dipolar relaxation during the formation of liquid droplets upon the interaction of virus capsid proteins with nucleic acids [74], and analyze the membrane wetting by biomolecular condensates [75].

In this article, we investigate the spectral properties of the ACDAN probe in two simple well-defined aqueous systems. Specifically, we analyzed the fluorescence spectral shifts in ACDAN in aqueous solutions containing kosmotropic and chaotropic salts from the Hofmeister series and in a confined system formed by agar hydrogel. Our aim was to understand how these distinct environments influence the response of the probe, shedding light on the water network and the solute interactions in both free and restricted aqueous media. The results reveal a significant shift in the emission band, which correlates with the

degree of order in the system under investigation. This finding suggests that the spectral response of ACDAN is highly sensitive to the structural organization of the surrounding environment, providing valuable insights into how molecular interactions and water structuring differ across varying conditions. This method is of relevance as it provides a simple and straightforward approach to analyzing the structural properties of water networks based on the sensitivity of fluorescence, with the possibility to easily analyze ongoing molecular processes in both solution and hydrogel by monitoring changes in the fluorescence signal.

## 2. Materials and Methods

### 2.1. Materials

Sodium dihydrogen phosphate ( $\text{Na}_2\text{HPO}_4$ ) (71640) was purchased from Merck, and sodium sulfate ( $\text{Na}_2\text{SO}_4$ ) (483007), sodium chloride ( $\text{NaCl}$ ) (479687), and sodium perchlorate ( $\text{NaClO}_4$ ) (482204) were purchased from Carlo Erba. Agar powder was purchased from Thermo Fisher Scientific (A10752.22). ACDAN (2-acetyl-6-(dimethylamino)naphthalene) (sc-208991) was purchased from Chem Cruz.

### 2.2. Sample Preparation

Hofmeister salt solution samples: All the solutions were prepared by dissolving the salts at three concentrations (1 M, 2 M, and 3 M) in Milli-Q water (18.2  $\text{M}\Omega\cdot\text{cm}$ ). The salt solutions were then filtered through a 0.2  $\mu\text{m}$  filter (VWR, 514-1274). ACDAN was added before the measurements at a concentration of 70  $\mu\text{M}$ . The measurements on the aqueous  $\text{Na}_2\text{HPO}_4$  solution were conducted on a stable supersaturated solution. Agar Hydrogel samples: Agar hydrogels were prepared by solubilizing the agar powder in Milli-Q water (18.2  $\text{M}\Omega\cdot\text{cm}$ ).

The concentration-dependent measurements were performed at different concentrations *wt/wt* (0.01%, 0.05%, 0.1%, 0.2%, 0.3%, 0.4%, 0.5%, 0.8%, 1.0%). In this case, the solutions were heated at 80 °C for 30 min and then cooled down at 45 °C for 30 min. The solutions were then transferred in PPMA semi-micro cuvettes, and ACDAN was added to a final concentration of 70  $\mu\text{M}$ . The solutions were cooled at 4 °C for 60 min to induce hydrogel formation then equilibrated at room temperature for 30 min before performing the measurements.

The time evolution of hydrogel formation was monitored on a sample consisting of the 0.5% *wt/wt* solution. In this case, the solution was heated at 80 °C for 30 min and then cooled at 45 °C for 30 min. The solutions for fluorescence analysis were then added with ACDAN to a final concentration of 70  $\mu\text{M}$ . Gel formation was observed during incubation at 20 °C for 250 min.

### 2.3. NIR Absorption Measurements

NIR absorption spectra were measured with a Jasco V770 spectrophotometer (Jasco, Tokiyo, Japan) equipped with a Jasco ETCR-762 Peltier cell as a temperature controller. A 1 mm path-length quartz cell has been used. The bandwidth was set to 8 nm, the response time to 0.24 s, the data interval to 0.5 nm, and the scan speed to 200 nm/min. All the solutions were prepared just before the measurements. The measurements performed on the salt solutions were conducted at room temperature, and spectra were normalized by the concentration of water in the solution. The kinetics measurements on the 0.5% *wt/wt* agar hydrogel were conducted at 20 °C, with spectra acquired every 5 min for 250 min.

### 2.4. Fluorescence Emission Measurements

Fluorescence spectra were acquired using a Jasco-FP-8500 spectrofluorometer (Jasco, Tokiyo, Japan) equipped with a Jasco ETC-815 Peltier cell as a temperature controller. The measurements on the salt solutions were performed at room temperature in a 1 cm path-length quartz cuvette. The spectra were acquired in the range of 370–650 nm, using  $\lambda_{\text{exc}} = 380$  nm with an excitation bandwidth of 10 nm, an emission bandwidth of 2.5 nm,

a response time of 1 s, a data interval of 0.5 nm, and a scan speed of 100 nm/min. The measurements on the agar gel were performed in a semi-micro PMMA cuvette. The spectra were acquired in the range 370–650 nm, using  $\lambda_{\text{exc}} = 380$  nm with an excitation bandwidth of 5 nm, an emission bandwidth of 2.5 nm, a response time of 1 s, a data interval of 0.5 nm, and a scan speed of 100 nm/min. The concentration-dependent measurements were acquired at room temperature after sample equilibration. The kinetics measurements were acquired at 20 °C during hydrogel maturation.

ACDAN fluorescence was analyzed in terms of the generalized polarization (GP) that was calculated using the expression adapted from Parassassi et al. [76] as follows:

$$GP = \frac{I_{475} - I_{550}}{I_{475} + I_{550}}, \quad (1)$$

where  $I_{475}$  and  $I_{550}$  are the fluorescence intensity at the corresponding wavelengths. The increase in the GP value indicates a spectral blueshift, while its decrease indicates a spectral redshift.

### 2.5. Rayleigh Scattering Measurements

Rayleigh scattering measurements were acquired using a Jasco-FP-8500 spectrofluorometer equipped with a Jasco ETC-815 Peltier cell as a temperature controller. Rayleigh scattering at 90° was registered as the maximum of the elastic peak of excitation light at 650 nm. A 2 mm path-length semi-micro quartz cuvette has been used. The excitation bandwidth was set to 5 nm, the emission bandwidth to 2.5 nm, the response time to 1 s, the data interval to 0.1 nm, and the scan speed to 100 nm/min.

## 3. Results

To elucidate the relationship between ACDAN fluorescence emissions and the H-bonding order of water, we present results from simple model systems that allow for the tuning of water's molecular order. Aqueous solutions containing kosmotropic and chaotropic sodium salts from the Hofmeister series were analyzed. The anions investigated in this study are  $\text{SO}_4^{2-}$ ,  $\text{HPO}_4^{2-}$ ,  $\text{Cl}^-$ , and  $\text{ClO}_4^-$ . Changes in the ACDAN fluorescence were studied in relation to changes in the overtone band of water in the NIR spectra. The peak centered at about 1450 nm is typically assigned to the overtone absorption of fundamental molecular vibrational modes of the O-H bond in water, and its changes can be related to alterations in the H-bond network order [17,54–58].

Figure 1a,b show NIR absorption spectra of  $\text{Na}_2\text{HPO}_4$  and  $\text{Na}_2\text{SO}_4$  solutions at increasing concentrations (from 1 M to 3 M) and the spectrum of water as a reference, measured in the range of 1300–1750 nm. Each spectrum is normalized to the water molecule mass concentration. Figure 1c,d show ACDAN steady-state fluorescence emission spectra of the same samples (including water) measured under excitation at  $\lambda_{\text{exc}} = 380$  nm in the range of 370–650 nm. Fluorescence spectra are normalized to the maximum intensity. The variation in these kosmotropic salt concentrations allows us to probe their impact on water structure, particularly their ability to enhance hydrogen bonding and promote order in the surrounding solvent environment.

The variations in the NIR spectra in Figure 1a,b can be related to the variation induced by those ions in the H-bonding structures. As can be seen, when the concentration of these salts increases, a decrease in the absorption band intensity is observed in both samples. Notably, it is accompanied by a shift towards longer wavelengths, and the emergence of a peak at 1475 nm becomes evident. The observed shift towards longer wavelengths indicates that, under the presented conditions, the presence of  $\text{HPO}_4^{2-}$  and  $\text{SO}_4^{2-}$  promotes a greater degree of water molecule structuring. The observed variations, in samples with the same salt concentration are more pronounced for  $\text{HPO}_4^{2-}$ .

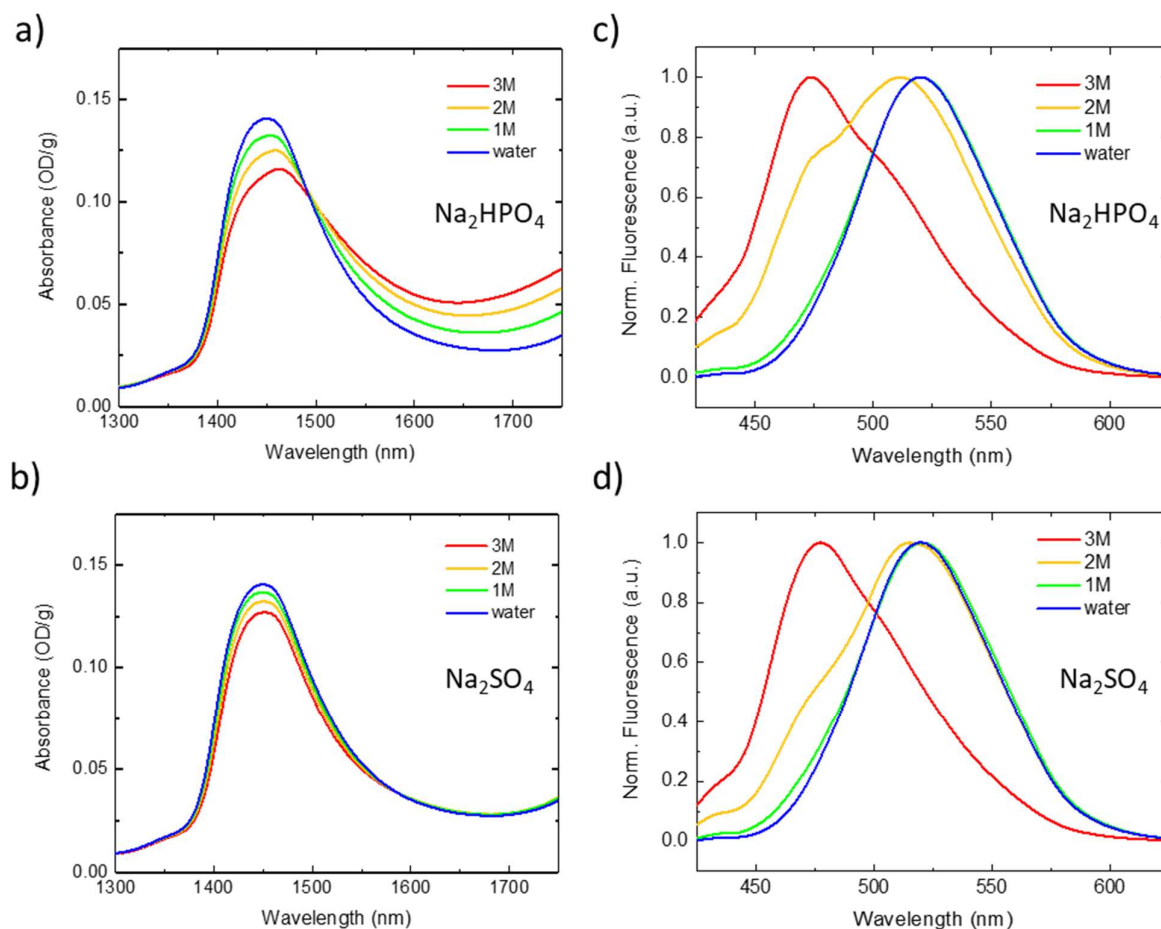


**Figure 1.** NIR absorbance of the water solution of kosmotropic salts of (a) sodium dihydrogen phosphate ( $\text{Na}_2\text{HPO}_4$ ) and (b) sodium sulfate ( $\text{Na}_2\text{SO}_4$ ) at 1 M, 2 M, and 3 M. The spectrum of pure water is reported for comparison. NIR spectra have been normalized by the water mass concentration. ACDAN fluorescence emission spectra in (c)  $\text{Na}_2\text{HPO}_4$  and (d)  $\text{Na}_2\text{SO}_4$  water solutions ( $\lambda_{\text{exc}} = 380$  nm, detection range = 370–650 nm). Fluorescence spectra have been normalized to the maximum intensity.

Figure 1c,d show ACDAN fluorescence emission spectra, normalized to their maximum intensity in  $\text{Na}_2\text{HPO}_4$  and  $\text{Na}_2\text{SO}_4$  aqueous solutions, respectively, at increasing concentrations. The spectrum of ACDAN in pure water is also reported. As can be observed for both kosmotropic salt solutions, changes in the shape of the ACDAN spectrum are observed, since a spectral component centered at about 475 nm grows as the salt concentration increases (this component is barely evident for 1 M samples but becomes much more pronounced for samples above 2 M). This translates into an overall blue shift in the fluorescence spectrum, which becomes more pronounced with the increasing molar concentration of the salts. In line with previous data, the spectral blue shift is more pronounced in the  $\text{Na}_2\text{HPO}_4$  solution with respect to the  $\text{Na}_2\text{SO}_4$  solution. Alongside the blue shift, the raw data show a decrease in intensity that correlates with the degree of order. However, at this stage, our interest is focused primarily on the band shape, which provides a significant and reliable fingerprint for fluorescence emission data. The observed blue shift is due to the reduction in the dielectric relaxation of the water molecules, as the kosmotropic agents strengthen the hydrogen-bonding network in water. The enhanced structuring of water molecules leads to a more rigid solvation shell around the probe. This result aligns with data obtained from more complex systems, where the ordering of water is provided by an increase in molecular crowding [72,73]. In such environments, the presence of macromolecules or other solutes can significantly alter the dynamics of water, leading

to enhanced hydrogen bonding and a more structured solvent network. As molecular crowding increases, water molecules are compelled to adopt a more organized arrangement around the solutes, which further impacts the solvation dynamics and, consequently, the behavior of molecular probes like ACDAN.

An opposite behavior is observed in solutions containing chaotropic salts. Figure 2a,b show NIR absorption spectra of NaCl and NaClO<sub>4</sub> solutions at increasing concentrations (from 1 M to 3 M) and the spectrum of water as a reference in the range 1300–1750 nm. Each spectrum is normalized to the water molecule concentration. Figure 2c,d show ACDAN steady-state fluorescence emission spectra of the same samples (including water) measured under excitation at  $\lambda_{\text{exc}} = 380$  nm in the range of 370–650 nm. Fluorescence spectra are normalized to the maximum intensity.

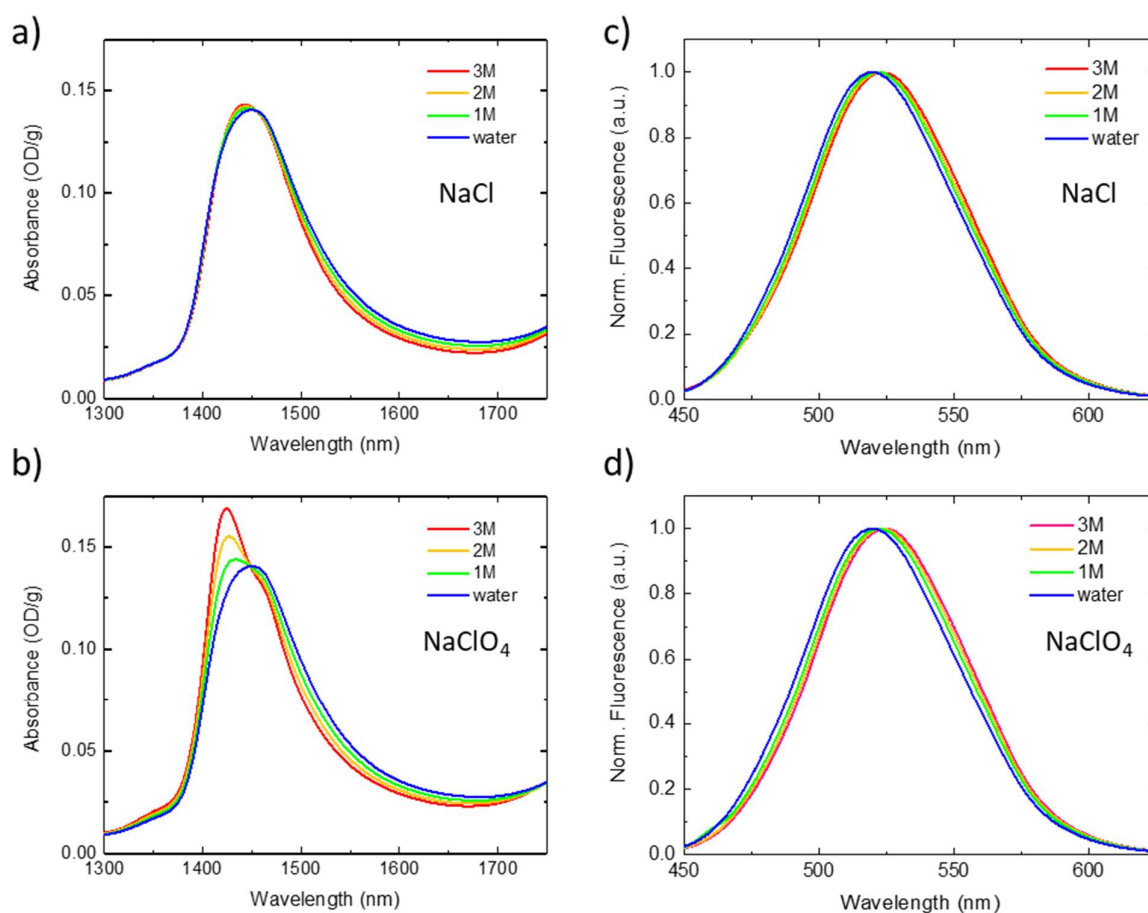


**Figure 2.** NIR absorbance of the water solution of chaotropic salts of (a) sodium chloride (NaCl) and (b) sodium perchlorate (NaClO<sub>4</sub>) at 1 M, 2 M, and 3 M. The spectrum of pure water is reported for comparison. NIR spectra have been normalized by the water mass concentration. ACDAN fluorescence emission spectra in (c) NaCl and (d) NaClO<sub>4</sub> water solutions ( $\lambda_{\text{exc}} = 380$  nm, detection range = 370–650 nm). Fluorescence spectra have been normalized to the maximum intensity.

For both chaotropic agents, a significant shift in the main peak towards lower wavelengths occurs as the salt concentration increases. The growth of a distinct peak emerging around 1410 nm is observed. The variation extent of this peak is more pronounced for the NaClO<sub>4</sub> solution. The observed spectral shift indicates a variation in the relative intensities of the absorption bands associated with different O-H groups within water clusters, each exhibiting differing degrees of hydrogen bonding. The observed shift results from an increase in the intensity of the shorter wavelength bands. This is consistent with the Hofmeister series, which underscores their role in disrupting the hydrogen-bonding network of water and altering the molecular order [25,27,28]. In Figure 2c,d, the normalized emission spectra

of ACDAN for the respective chaotropic salt solutions are presented as a function of concentration. In this case, the emission spectra exhibit a small red shift for all three salts as their concentrations increase. In the presence of chaotropic agents, results suggest that the dye exhibits limited capability in monitoring further increases in dielectric relaxation compared to a pure water sample. This may be attributed to the fact that water molecules in pure water samples are already sufficiently mobile to be rearranged and reoriented by ACDAN dipoles, thereby reducing the influence of chaotropic agents in this instance. However, although the variations are quite small, it is noteworthy that the red shift demonstrated by ACDAN fluorescence is concentration-dependent, underlying the significant effect of chaotropic ions. Furthermore, the behavior is the opposite of what occurs in solutions containing kosmotropic salts. In kosmotropic environments, the increased water structuring leads to a blue shift in fluorescence emission, while in chaotropic solutions, the disruption of the hydrogen-bonding network results in a red shift. The opposing behavior underscores the distinct ways in which these two classes of salts influence the molecular organization of water. Although these small spectral changes can provide valuable insights into the nature of solute–water interactions and their effects on the surrounding environment, the ACDAN probe appears to be more sensitive to variations that tend to increase the order within the system.

In addition to the analysis of the water network in solutions of salts with different ordering/disordering behavior, the dynamics of water have been investigated in agar hydrogels as well, providing insights into both the structure of water in the hydrogel itself and the during the gelation process. In this case, spectral changes in the fluorescence signal of ACDAN successfully allowed for the monitoring of water dynamics and its ordering during gelation. By cooling a hot agar solution, a 3D polymeric network is formed that entraps the solvent to produce a hydrogel. Agar hydrogel provides an ideal model system for studying water structure in confined environments, as its matrix mimics the restricted spaces found in biological systems [77]. The water within the hydrogel experiences a different hydrogen-bonding network compared to bulk water, due to the spatial constraints imposed by the gel matrix [34–36]. Water molecules may either move freely around the agar macromolecules or interact with agar macromolecules by hydrogen bonding. As the agar concentration increases, the number of agar molecules available for hydrogen bonding also increases. Furthermore, the increase in agar concentration parallels with the reduction in the average pores size of the hydrogel matrix [78,79].

Due to its sensitivity to local dielectric relaxation, ACDAN is particularly well suited for probing such systems. In agar hydrogel, the fluorescence properties of ACDAN indeed can reveal changes in water dynamics and the degree of molecular ordering caused by constraints imposed by agar matrices. Figure 3a presents the normalized fluorescence emission spectra of ACDAN in agar hydrogels at different concentrations. The ACDAN fluorescence spectrum in pure water is included for comparison. As the agar concentration increases, a clear broadening of the emission band is observed, accompanied by a significant blue shift towards shorter wavelengths. This shift suggests that the confinement of water within the agar hydrogel matrix induces significant changes in the local environment surrounding the ACDAN probe, likely due to the increased molecular ordering of water as the gel's density rises.

As shown in Figure 3b, we analyzed the spectra in terms of the generalized polarization (GP) to quantify the shift in the ACDAN fluorescence spectra. GP was calculated following the expression introduced by Parassasi et al. [76] using the fluorescence intensity at 475 nm and 550 nm. GP is a well-established parameter for analyzing spectral changes in several dyes of the DAN family [73,80–84]. This parameter reflects the degree of dipolar relaxation experienced by the probe. Initially designed to study relaxation effects in membranes for LAURDAN, it has since been generalized for ACDAN as well.



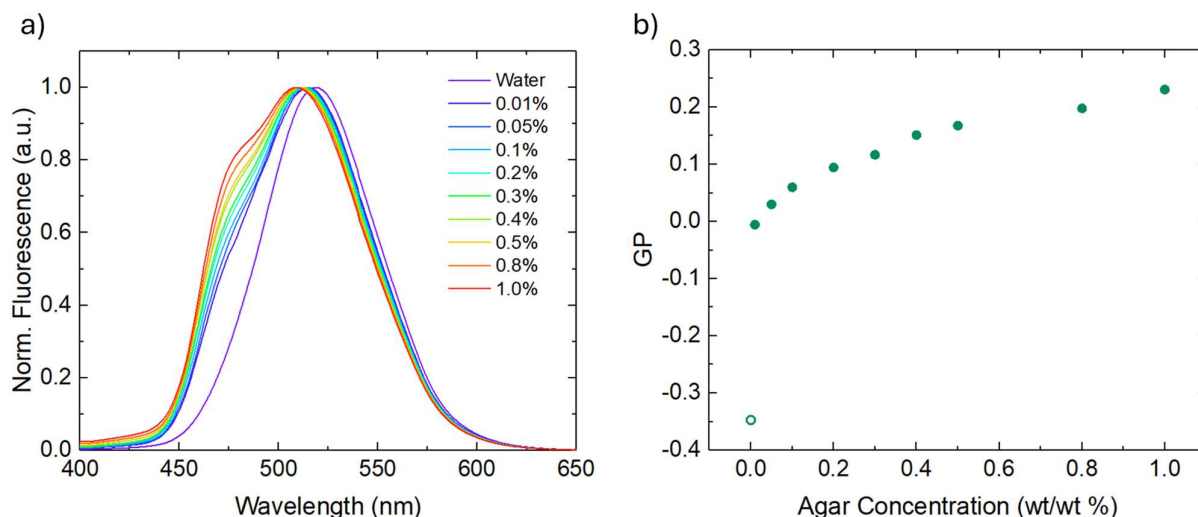


**Figure 3.** (a) ACDAN fluorescence emission spectra ( $\lambda_{\text{exc}} = 380$  nm, detection range = 370–650 nm) measured in agar hydrogels as a function of agar concentration ranging from 0.01% to 1.0% (*wt/wt*). ACDAN fluorescence emission spectrum in water is reported as well. Fluorescence spectra have been normalized to the maximum intensity. (b) GP analysis of the ACDAN fluorescence emission band, measured at 475 nm and 550 nm. The empty green circle is the GP value calculated from the water spectrum.

For instance, GP has been used to distinguish different regions within the stoma of the plant *Arabidopsis thaliana* due to the varying dipolar relaxation experienced by ACDAN [70]. Similarly, GP has also been applied to investigate the spectral changes in ACDAN during glycolytic oscillations in yeast cells [71]. In general, the increase in the GP indicates a spectral blue shift while the decrease denotes a spectral red shift. The GP value for pure water is negative (reported in the plot as an empty green circle), and as the concentration of agar in the gel increases, the GP shifts toward positive values.

The fluorescence spectrum of ACDAN in pure water shows a single component centered around 520 nm, yielding a negative GP value. Upon adding agar, a second blue-shifted component appears around 475 nm, indicating increased water ordering and resulting in positive GP values. To explore this spectral change in studying agar gelation in water, we selected an agar concentration range suitable for observing the gelation process, starting from concentrations where agar chains remain in the solution to those forming firm hydrogels. Since agar typically gels in water at 0.5% *w/w* [85,86], concentrations from 0.01% to 1% were chosen to investigate both non-gelling and gelling states. In the analysis of the GP as a function of agar concentration, a relevant spectral change was observed to already be moving from pure water to the first agar 0.01% *wt/wt* solution. Such a change likely results from the notable agar presence compared to pure water, with this concentration being high enough to significantly influence water ordering.

The shift in the GP indicates a reduction in the dielectric relaxation of the water network, resulting from a more ordered structure. This shift indicates that water structuring occurs at a higher agar content, as the restricted environment within the gel network forces water molecules into more ordered arrangements. ACDAN fluorescence emission in bulk water is characterized by a narrow peak centered at 520 nm in line with what is reported in the literature [71]. The resulting negative GP reflects how water experiences less molecular constraint.

To gain more information on the system in analysis, the time evolution of the ACDAN fluorescence emission spectrum was monitored during hydrogel formation at 20 °C from a 0.5% agar solution. This experiment aimed to capture dynamic changes in the water network due to the changes in molecular interactions occurring during agar polymerization. This temporal analysis is crucial for understanding the stability and adaptability of the water structure in hydrogel environments, providing further insights into how these

changes may influence biophysical and biochemical processes that are relevant to cellular behavior and material applications. Figure 4 reports the time evolution of agar hydrogel formation conducted at 20 °C on a solution at 0.5% *wt/wt* agar concentration for 250 min. Hydrogel was prepared as described in the methods. Figure 4a shows the kinetics of Rayleigh scattering data measured at 650 nm, i.e., a wavelength at which no fluorescence signal is present from the sample. In Figure 4b, the kinetics of ACDAN fluorescence spectra are reported. Fluorescence spectra are normalized to their maximum. Figure 4c shows the GP calculated at 475 nm and 550 nm as a function of time. In Figure 4d, the differential NIR absorbance spectra of the 1450 nm water band are reported to highlight the variation in the NIR absorbance spectra during the gelation process. Figure 4e shows the maximum of the differential NIR absorbance spectra as a function of time.

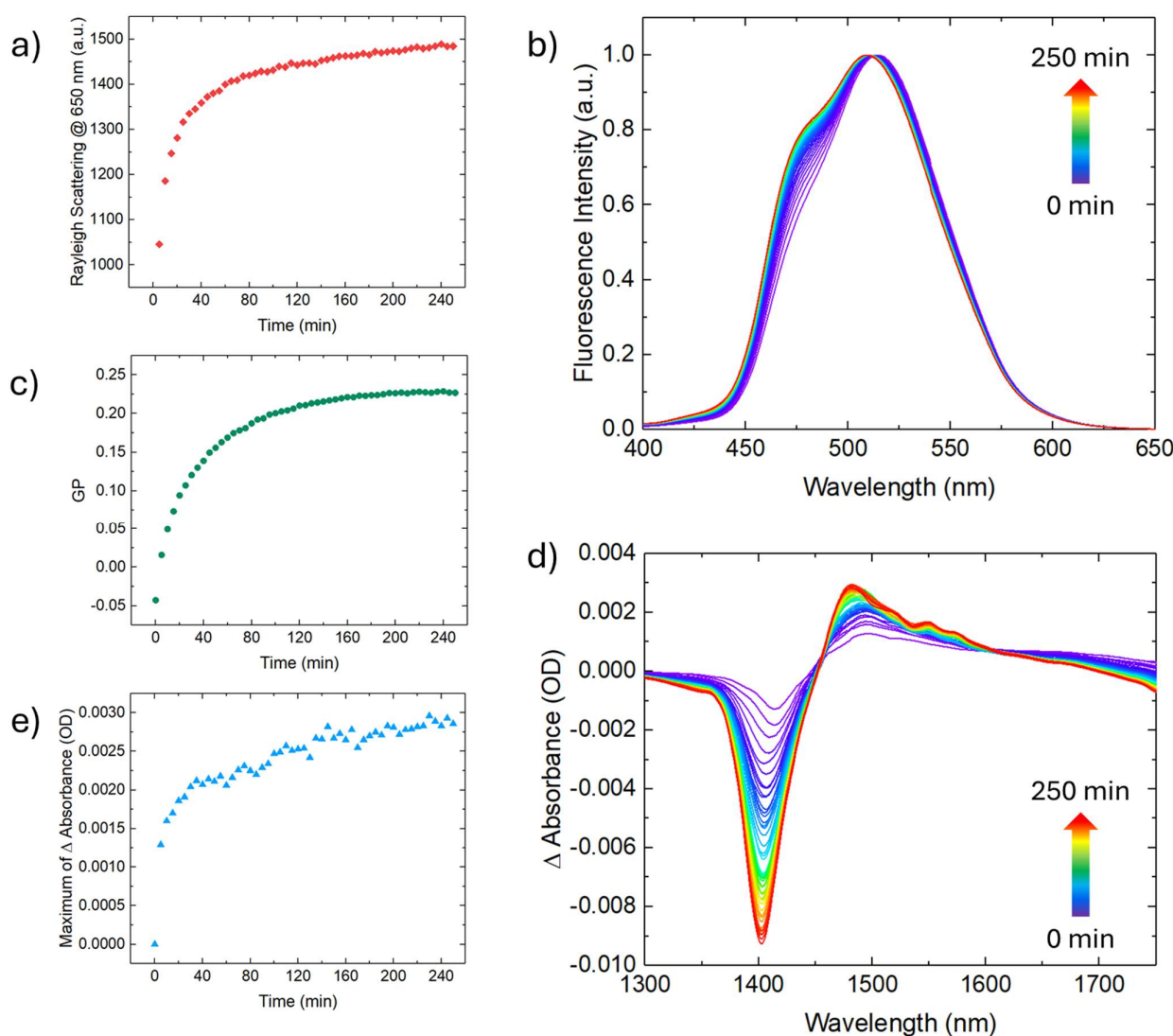


**Figure 4.** Time evolution of hydrogel formation was monitored on a sample consisting of a 0.5% *wt/wt* agar solution for 250 min. (a) Rayleigh scattering of the sample measured at 650 nm during 20 °C thermal gelification. (b) ACDAN fluorescence emission spectra as a function of time ( $\lambda_{exc} = 380$  nm, detection range = 370–650 nm). Fluorescence spectra have been normalized to the maximum intensity. (c) GP analysis of the ACDAN fluorescence emission band, calculated at 475 nm and 550 nm as a function of time. (d) Differential spectra of the 1450 nm NIR absorption band. (e) Maximum of the differential NIR spectra as a function of time.

The Rayleigh scattering signal is observed to grow as a function of time, reaching a plateau in about 1 h. This indicates the occurrence of the progressive polymerization of

agar and hydrogel formation [87,88]. At the same time scale, the ACDAN fluorescence signal undergoes a blue shift in line with previous observations in salt solutions and agar hydrogels. The observed blue shift indicates the change in the ACDAN local environment, which can be attributed to the progressive reorganization of the hydrogen-bonding network occurring during hydrogel maturation. The time evolution of fluorescence emission is better highlighted by the GP in panel c, where a monotonic growth to a maximum is evident, which parallels the time evolution of scattering measurements. It is worth noting that the value of the first GP point is negative, in line with the GP value of pure water, as shown in Figure 3. This value suggests that at the beginning of the time evolution, when the hydrogel has not yet formed, ACDAN experiences an environment analogous to pure water, characterized by high molecule mobility. This environment progressively changes towards a higher rigidity, which is translated in the blue shift in the ACDAN fluorescence band and consequently to an increase in the GP values. The analysis of the NIR water band reported in Figure 4d shows significant differences over time. Specifically, the differential spectra show a reduction in the component centered at about 1410 nm, together with the growth of a component around 1475 nm. In line with the related literature [39,89], the observed spectral shift highlights the progressive formation and maturation of the hydrogel. These processes are complemented by the ordering of the hydrogen-bonding network of water.

The maximum of the 1475 nm component over time, reported in Figure 4e, presents larger fluctuations with respect to the GP and ACDAN data. These fluctuations are dictated by the small variations observed in the differential NIR absorption spectra, which are approximately in the order of magnitude of  $10^{-3}$  OD. Although these variations are very small, the data are extremely relevant as their trend parallels well the scattering and GP trends (See Supplementary Materials Figure S2), highlighting the clear trend in the process and emphasizing the role of water organization in the overall gelation process.

Reported experiments underline the dynamic evolution of the structural organization occurring within the gel matrix. The concurrent rise in the GP and differential NIR absorbance indicates an enhancement in the ordering of the hydrogen-bonding network as the gelation process progresses. Collectively, these findings provide compelling evidence of the intricate relationships between ACDAN's emission properties, the structural maturation of the gel, and the underlying molecular interactions within the confined aqueous environment.

#### 4. Conclusions

This study explores the molecular interactions and structural organization of water using ACDAN fluorescence dye as a molecular probe. We analyze the emission fluorescence of ACDAN in aqueous solutions containing kosmotropic and chaotropic salts from the Hofmeister series, as well as in agar hydrogel matrices, with the aim to investigate how the water hydrogen-bonding network can be explored and monitored at the molecular level by spectral changes in the ACDAN fluorescence. Our findings reveal that kosmotropic salts, which enhance water structuring, lead to a significant blue shift in ACDAN fluorescence emission spectra. This shift highlights the role of these salts in fostering a more ordered hydrogen-bonding network and reducing dielectric relaxation, which is crucial for various biochemical and technological processes. In contrast, chaotropic salts, which disrupt the hydrogen-bonding network, result in red shifts in the emission spectra and highlight the different mechanisms by which these solutes influence water dynamics. These spectral shifts are consistent with the results obtained by NIR absorption spectroscopy. Indeed, NIR spectroscopy detected changes in water molecule vibrations, providing information into the rearrangement of the H-bonding network in the presence of kosmotropic and chaotropic salts. This complementary approach enables a deeper characterization of the molecular interactions affecting the H-bond network of water and dipolar relaxation dynamics. The analysis of ACDAN in confined agar hydrogel systems revealed further complexities in water's structural organization. The confinement induced by the hydrogel matrix led to significant changes in the local water organization, promoting greater structuring, as

reflected in the ACDAN fluorescence emission and NIR absorption data. The analysis of gelation also demonstrated how the structural organization of water evolves over time, providing a dynamic view of the water network's maturation. Overall, this study emphasizes the critical role of water's molecular interactions in shaping the ACDAN fluorescence behavior in the presence of solutes and macromolecules in both free and confined environments. The results confirm the potential of this dye for monitoring water's dielectric relaxation and structural organization in response to molecular interactions. Understanding these interactions not only enhances our comprehension of fundamental biochemical processes, but also informs the design of materials and systems where water plays a pivotal role. Future research can build upon these findings by exploring additional environmental factors and conditions that influence water's structural dynamics, further elucidating its implications for biological and chemical systems of technological relevance.

**Supplementary Materials:** The following supporting information can be downloaded at <https://www.mdpi.com/article/10.3390/biophysica4040041/s1>, Figure S1: (a) Chemical structure of 2-acetyl-6-(dimethylamino)naphthalene (ACDAN). (b) Simplified Jablonski diagram for the ACDAN molecule: the absorption transition (purple arrow) brings the molecule from the ground state to the excited state, where it couples with the water molecules. If the coupling is weak and ACDAN experiences a low dipolar relaxation, due to an ordered water state, the excited state does not lose energy and the emitted photon is more energetic (blue arrow). If ACDAN experiences a higher dipolar relaxation, due to a more disordered state of water molecules and their consequent rearrangement and reorientation towards the ACDAN dipole, its excited state loses more energy and the emitted photon is less energetic (green arrow); Figure S2: Time evolution of hydrogel formation monitored on a sample consisting of a 0.5% *wt/wt* agar solution for 250 min during 20 °C thermal gelification. Superimposed data of Rayleigh scattering of the sample measured at 650 nm (gray triangles), GP of ACDAN fluorescence emission spectra (cyan circles), and maximum of the differential spectra of the 1450 nm NIR absorption band (red circles).

**Author Contributions:** Conceptualization, V.V. and G.S.; methodology, G.D.L., V.F., V.V. and G.S.; formal analysis, G.D.L., V.F., V.V. and G.S.; investigation, G.D.L., V.F. and G.S.; resources, V.V. and B.P.; data curation, G.D.L., V.F., V.V. and G.S.; writing—original draft preparation, G.D.L., V.V. and G.S.; writing—review and editing, G.D.L., V.F., B.P., V.V. and G.S.; supervision, V.V. and G.S.; funding acquisition, V.V. and B.P. All authors have read and agreed to the published version of the manuscript.

**Funding:** This researcher received funding from MUR—PRIN PNRR—LLPS (Liquid–Liquid Phase Separation Dynamics in Biomimetic Compartments) and FFR Unipa 2023 and FFR Unipa 2024. This work received funding from “Network 4 Energy Sustainable Transition—NEST” B73C22001280006 (project funded under the National Recovery and Resilience Plan (NRRP), Mission 4 Component 2 Investment 1.3—funded by the European Union—NextGenerationEU). “Consorzio Interuniversitario Nazionale per la Scienza e Tecnologia dei Materiali” (INSTM) is acknowledged for the three-year project “Printed surfaces and micro-compartments for advanced technologies”.

**Data Availability Statement:** The datasets used and/or analyzed during the current study are available from the corresponding author upon reasonable request.

**Acknowledgments:** The authors acknowledge Maurizio Leone for useful comments and discussions.

**Conflicts of Interest:** The authors declare no conflicts of interest.

## References

1. Bellissent-Funel, M.C.; Hassanali, A.; Havenith, M.; Henchman, R.; Pohl, P.; Sterpone, F.; Van Der Spoel, D.; Xu, Y.; Garcia, A.E. Water Determines the Structure and Dynamics of Proteins. *Chem. Rev.* **2016**, *116*, 7673–7697. [[CrossRef](#)]
2. Pezzotti, S.; König, B.; Ramos, S.; Schwaab, G.; Havenith, M. Liquid-Liquid Phase Separation? Ask the Water! *J. Phys. Chem. Lett.* **2023**, *14*, 1556–1563. [[CrossRef](#)]
3. Zaslavsky, B.Y.; Uversky, V.N. In Aqua Veritas: The Indispensable yet Mostly Ignored Role of Water in Phase Separation and Membrane-Less Organelles. *Biochemistry* **2018**, *57*, 2437–2451. [[CrossRef](#)]
4. Chaplin, M. Do We Underestimate the Importance of Water in Cell Biology? *Nat. Rev. Mol. Cell Biol.* **2006**, *7*, 861–866. [[CrossRef](#)]
5. Ribeiro, S.S.; Samanta, N.; Ebbinghaus, S.; Marcos, J.C. The Synergic Effect of Water and Biomolecules in Intracellular Phase Separation. *Nat. Rev. Chem.* **2019**, *3*, 552–561. [[CrossRef](#)]

6. Weinhold, F. Resonance Character of Hydrogen-Bonding Interactions in Water and Other H-Bonded Species. *Adv. Protein Chem.* **2005**, *72*, 121–155.
7. Song, Y.; Chen, H.; Zhang, C.; Zhang, Y.; Yin, Y. Characteristics of Hydrogen Bond Revealed from Water Clusters. *Eur. Phys. J. D* **2014**, *68*, 242. [[CrossRef](#)]
8. Ball, P. Water as an Active Constituent in Cell Biology. *Chem. Rev.* **2008**, *108*, 74–108. [[CrossRef](#)]
9. Laage, D.; Elsaesser, T.; Hynes, J.T. Water Dynamics in the Hydration Shells of Biomolecules. *Chem. Rev.* **2017**, *117*, 10694–10725. [[CrossRef](#)]
10. Dér, A.; Kelemen, L.; Fábrián, L.; Taneva, S.G.; Fodor, E.; Páli, T.; Cupane, A.; Cacace, M.G.; Ramsden, J.J. Interfacial Water Structure Controls Protein Conformation. *J. Phys. Chem. B* **2007**, *111*, 5344–5350. [[CrossRef](#)]
11. Levy, Y.; Onuchic, J.N. Water mediation in protein folding and molecular recognition. *Annu. Rev. Biophys. Biomol. Struct.* **2006**, *35*, 389–415. [[CrossRef](#)]
12. Mukherjee, S.; Chowdhury, P.; Gai, F. Effect of Dehydration on the Aggregation Kinetics of Two Amyloid Peptides. *J. Phys. Chem. B* **2009**, *113*, 531–535. [[CrossRef](#)]
13. Privalov, P.L.; Crane-Robinson, C. Role of Water in the Formation of Macromolecular Structures. *Eur. Biophys. J.* **2017**, *46*, 203–224. [[CrossRef](#)]
14. Vetri, V.; Piccirilli, F.; Krausser, J.; Buscarino, G.; Łapińska, U.; Vestergaard, B.; Zaccone, A.; Foderà, V. Ethanol Controls the Self-Assembly and Mesoscopic Properties of Human Insulin Amyloid Spherulites. *J. Phys. Chem. B* **2018**, *122*, 3101–3112. [[CrossRef](#)]
15. Shiraga, K.; Ogawa, Y.; Kondo, N. Hydrogen Bond Network of Water around Protein Investigated with Terahertz and Infrared Spectroscopy. *Biophys. J.* **2016**, *111*, 2629–2641. [[CrossRef](#)]
16. Zupančič, B.; Grdadolnik, J. Solute-Induced Changes in the Water H-Bond Network of Different Alcohol-Aqueous Systems. *J. Mol. Liq.* **2021**, *341*, 117349. [[CrossRef](#)]
17. Andaloro, G.; Leone, M. Structural Properties of Aqueous Electrolyte Solutions from i.r. Absorption Spectra. *Il Nuovo Cimento D* **1985**, *5*, 133–146. [[CrossRef](#)]
18. Smith, J.D.; Cappa, C.D.; Wilson, K.R.; Cohen, R.C.; Geissler, P.L.; Saykally, R.J. Unified Description of Temperature-Dependent Hydrogen-Bond Rearrangements in Liquid Water. *Proc. Natl. Acad. Sci. USA* **2005**, *102*, 14171–14174. [[CrossRef](#)]
19. Yang, B.; Ren, P.; Xing, L.; Wang, S.; Sun, C. Roles of Hydrogen Bonding Interactions and Hydrophobic Effects on Enhanced Water Structure in Aqueous Solutions of Amphiphilic Organic Molecules. *Spectrochim. Acta A Mol. Biomol. Spectrosc.* **2023**, *296*, 122605. [[CrossRef](#)]
20. Stahl, N.; Jencks, W.P. Hydrogen Bonding between Solutes in Aqueous Solution. *J. Am. Chem. Soc.* **1986**, *108*, 4196–4205. [[CrossRef](#)]
21. Abbasi, A.; Lindqvist-Reis, P.; Eriksson, L.; Sandström, D.; Lidin, S.; Persson, I.; Sandström, M. Highly Hydrated Cations: Deficiency, Mobility, and Coordination of Water in Crystalline Nonahydrated Scandium(III), Yttrium(III), and Lanthanoid(III) Trifluoromethanesulfonates. *Chem.—A Eur. J.* **2005**, *11*, 4065–4077. [[CrossRef](#)]
22. Soper, A.K.; Weckström, K. Ion Solvation and Water Structure in Potassium Halide Aqueous Solutions. *Biophys. Chem.* **2006**, *124*, 180–191. [[CrossRef](#)]
23. Acharyya, A.; Mukherjee, D.; Gai, F. Assessing the Effect of Hofmeister Anions on the Hydrogen-Bonding Strength of Water via Nitrile Stretching Frequency Shift. *J. Phys. Chem. B* **2020**, *124*, 11783–11792. [[CrossRef](#)]
24. O'Brien, J.T.; Williams, E.R. Effects of Ions on Hydrogen-Bonding Water Networks in Large Aqueous Nanodrops. *J. Am. Chem. Soc.* **2012**, *134*, 10228–10236. [[CrossRef](#)]
25. Marcus, Y. Effect of Ions on the Structure of Water: Structure Making and Breaking. *Chem. Rev.* **2009**, *109*, 1346–1370. [[CrossRef](#)]
26. Zhang, Y.; Cremer, P.S. Interactions between Macromolecules and Ions: The Hofmeister Series. *Curr. Opin. Chem. Biol.* **2006**, *10*, 658–663. [[CrossRef](#)]
27. Kunz, W.; Henle, J.; Ninham, B.W. “Zur Lehre von Der Wirkung Der Salze” (about the Science of the Effect of Salts): Franz Hofmeister’s Historical Papers. *Curr. Opin. Colloid Interface Sci.* **2004**, *9*, 19–37. [[CrossRef](#)]
28. Kang, B.; Tang, H.; Zhao, Z.; Song, S. Hofmeister Series: Insights of Ion Specificity from Amphiphilic Assembly and Interface Property. *ACS Omega* **2020**, *5*, 6229–6239. [[CrossRef](#)]
29. Ferreira, L.A.; Uversky, V.N.; Zaslavsky, B.Y. Effects of the Hofmeister Series of Sodium Salts on the Solvent Properties of Water. *Phys. Chem. Chem. Phys.* **2017**, *19*, 5254–5261. [[CrossRef](#)]
30. Lo Nostro, P.; Ninham, B.W. Hofmeister Phenomena: An Update on Ion Specificity in Biology. *Chem. Rev.* **2012**, *112*, 2286–2322. [[CrossRef](#)]
31. Chakraborty, S.; Kumar, H.; Dasgupta, C.; Maiti, P.K. Confined Water: Structure, Dynamics, and Thermodynamics. *Acc. Chem. Res.* **2017**, *50*, 2139–2146. [[CrossRef](#)] [[PubMed](#)]
32. Cammarata, M.; Levantino, M.; Cupane, A.; Longo, A.; Martorana, A.; Bruni, F. Structure and Dynamics of Water Confined in Silica Hydrogels: X-Ray Scattering and Dielectric Spectroscopy Studies. *Eur. Phys. J. E* **2003**, *12*, 63–66. [[CrossRef](#)] [[PubMed](#)]
33. Belovolova, L.V.; Glushkov, M.V. Porous Matrices and Specific Features of Water in Nanostructures. *Phys. Wave Phenom.* **2021**, *29*, 249–277. [[CrossRef](#)]
34. Hechter, O.; Wittstruck, T.; McNiven, N.; Lester, G. Modification of the structure of water in agar gels. *Proc. Natl. Acad. Sci. USA* **1960**, *46*, 783–787. [[CrossRef](#)]
35. Gun’ko, V.M.; Savina, I.N.; Mikhalovsky, S.V. Properties of Water Bound in Hydrogels. *Gels* **2017**, *3*, 37. [[CrossRef](#)]

36. Boral, S.; Bohidar, H.B. Effect of Water Structure on Gelation of Agar in Glycerol Solutions and Phase Diagram of Agar Organogels. *J. Phys. Chem. B* **2012**, *116*, 7113–7121. [[CrossRef](#)]
37. Jhon, M.S.; Andrade, J.D. Water and Hydrogels. *J. Biomed. Mater. Res.* **1973**, *7*, 509–522. [[CrossRef](#)]
38. Bagchi, B. The Freezing of Water into Ice. In *Water in Biological and Chemical Processes*; Cambridge University Press (CUP): Cambridge, UK, 2013.
39. Ma, B.; Cai, W.; Shao, X. Analyzing the Water Confined in Hydrogel Using Near-Infrared Spectroscopy. *Appl. Spectrosc.* **2022**, *76*, 773–782. [[CrossRef](#)]
40. Zapanta, M.J.; Postelmans, A.; Saeys, W. Assessing the Hydration State of Agarose-Based Hydrogels Using Terahertz Spectroscopy. In Proceedings of the Terahertz Photonics II, Strasbourg, France, 31 May 2022.
41. Rossi, B.; Venuti, V.; D’Amico, F.; Gessini, A.; Castiglione, F.; Mele, A.; Punta, C.; Melone, L.; Crupi, V.; Majolino, D.; et al. Water and Polymer Dynamics in a Model Polysaccharide Hydrogel: The Role of Hydrophobic/Hydrophilic Balance. *Phys. Chem. Chem. Phys.* **2015**, *17*, 963–971. [[CrossRef](#)]
42. Pasqui, D.; De Cagna, M.; Barbucci, R. Polysaccharide-Based Hydrogels: The Key Role of Water in Affecting Mechanical Properties. *Polymers* **2012**, *4*, 1517–1534. [[CrossRef](#)]
43. Ball, P. Water Is an Activematrix of Life for Cell and Molecular Biology. *Proc. Natl. Acad. Sci. USA* **2017**, *114*, 13327–13335. [[CrossRef](#)] [[PubMed](#)]
44. Dargaville, B.L.; Hutmacher, D.W. Water as the Often Neglected Medium at the Interface between Materials and Biology. *Nat. Commun.* **2022**, *13*, 4222. [[CrossRef](#)] [[PubMed](#)]
45. Fouzri, A.; Dorbez-Sridi, R.; Oumezzine, M. Water Confined in Silica Gel and in Vycor Glass at Low and Room Temperature, X-ray Diffraction Study. *J. Chem. Phys.* **2002**, *116*, 791–797. [[CrossRef](#)]
46. De Michele, V.; Romanelli, G.; Cupane, A. Dynamics of Supercooled Confined Water Measured by Deep Inelastic Neutron Scattering. *Front. Phys.* **2018**, *13*, 138205. [[CrossRef](#)]
47. Fomina, M.; Schirò, G.; Cupane, A. Hydration Dependence of Myoglobin Dynamics Studied with Elastic Neutron Scattering, Differential Scanning Calorimetry and Broadband Dielectric Spectroscopy. *Biophys. Chem.* **2014**, *185*, 25–31. [[CrossRef](#)]
48. Otting, G.; Wüthrich, K. Studies of Protein Hydration in Aqueous Solution by Direct NMR Observation of Individual Protein-Bound Water Molecules. *J. Am. Chem. Soc.* **1989**, *111*, 1871–1875. [[CrossRef](#)]
49. Falourd, X.; Rondeau-Mouro, C.; Cambert, M.; Lahaye, M.; Chabbert, B.; Aguié-Béghin, V. Assessing the Complementarity of Time Domain NMR, Solid-State NMR and Dynamic Vapor Sorption in the Characterization of Polysaccharide-Water Interactions. *Carbohydr. Polym.* **2024**, *326*, 121579. [[CrossRef](#)]
50. Vishwam, T.; Aishwarya, K.; Prasad, T.V.; Joseph, A.; Raju, K.C.J. Dielectric Relaxation Spectroscopy of L-Proline Aqueous Solutions: Analysis of Relaxation Time and the Contribution of the Hydration Water. In *AIP Conference Proceedings*; AIP Publishing: Melville, NY, USA, 2024; Volume 2995.
51. Skinner, J.L.; Pieniazek, P.A.; Gruenbaum, S.M. Vibrational Spectroscopy of Water at Interfaces. *Acc. Chem. Res.* **2012**, *45*, 93–100. [[CrossRef](#)]
52. Li, D.; Zhu, Z.; Sun, D.W. Quantification of Hydrogen Bonding Strength of Water in Saccharide Aqueous Solutions by Confocal Raman Microscopy. *J. Mol. Liq.* **2021**, *342*, 117498. [[CrossRef](#)]
53. Tsenkova, R.; Kovacs, Z.; Kubota, Y. Aquaphotonics: Near Infrared Spectroscopy and Water States in Biological Systems. In *Membrane Hydration*; Springer: Cham, Switzerland, 2015; Volume 71. [[CrossRef](#)]
54. Chen, Y.; Ozaki, Y.; Czarniecki, M.A. Molecular Structure and Hydrogen Bonding in Pure Liquid Ethylene Glycol and Ethylene Glycol-Water Mixtures Studied Using NIR Spectroscopy. *Phys. Chem. Chem. Phys.* **2013**, *15*, 18694–18701. [[CrossRef](#)]
55. Wu, Z.; Ouyang, G.; Shi, X.; Ma, Q.; Wan, G.; Qiao, Y. Absorption and Quantitative Characteristics of C-H Bond and O-H Bond of NIR. *Opt. Spectrosc.* **2014**, *117*, 703–709. [[CrossRef](#)]
56. Andaloro, G.; Chiricò, P.; Guzzio, G.; Leone, M.; Palma-Vittorelli, M.B. Thermal Behavior of the near Ir Absorption of H<sub>2</sub>O and NaClO<sub>4</sub> Aqueous Solutions. *J. Chem. Phys.* **1976**, *66*, 335–341. [[CrossRef](#)]
57. Renati, P.; Kovacs, Z.; De Ninno, A.; Tsenkova, R. Temperature Dependence Analysis of the NIR Spectra of Liquid Water Confirms the Existence of Two Phases, One of Which Is in a Coherent State. *J. Mol. Liq.* **2019**, *292*, 111449. [[CrossRef](#)]
58. Weyer, L.G.; Lo, S.-C. Spectra–Structure Correlations in the Near-Infrared. In *Handbook of Vibrational Spectroscopy*; Wiley: Hoboken, NJ, USA, 2001.
59. Segtnan, V.H.; Šašić, Š.; Isaksson, T.; Ozaki, Y. Studies on the Structure of Water Using Two-Dimensional near-Infrared Correlation Spectroscopy and Principal Component Analysis. *Anal. Chem.* **2001**, *73*, 3153–3161. [[CrossRef](#)]
60. Uchida, N.; Yoshimura, N.; Takayanagi, M. Variation of the Near-Infrared Spectrum of Water from Dissolved Salts. *J. Solut. Chem.* **2015**, *44*, 2167–2178. [[CrossRef](#)]
61. Guo, Y.; Bae, J.; Fang, Z.; Li, P.; Zhao, F.; Yu, G. Hydrogels and Hydrogel-Derived Materials for Energy and Water Sustainability. *Chem. Rev.* **2020**, *120*, 7642–7707. [[CrossRef](#)]
62. Li, L.; Liu, Z.; Qi, R. Molecular Dynamics Simulations in Hydrogel Research and Its Applications in Energy Utilization: A Review. *Energy Rev.* **2024**, *3*, 100072. [[CrossRef](#)]
63. Li, L.; Wu, P.; Yu, F.; Ma, J. Double Network Hydrogels for Energy/Environmental Applications: Challenges and Opportunities. *J. Mater. Chem. A Mater.* **2022**, *10*, 9215–9247. [[CrossRef](#)]

64. Murphy, N.P.; Lampe, K.J. Mimicking Biological Phenomena in Hydrogel-Based Biomaterials to Promote Dynamic Cellular Responses. *J. Mater. Chem. B* **2015**, *3*, 7867–7880. [[CrossRef](#)]
65. Segura Zarate, A.Y.; Gontrani, L.; Galliano, S.; Bauer, E.M.; Donia, D.T.; Barolo, C.; Bonomo, M.; Carbone, M. Green Zinc/Galactomannan-Based Hydrogels Push up the Photovoltage of Quasi Solid Aqueous Dye Sensitized Solar Cells. *Sol. Energy* **2024**, *272*, 112460. [[CrossRef](#)]
66. Galliano, S.; Bella, F.; Bonomo, M.; Viscardi, G.; Gerbaldi, C.; Boschloo, G.; Barolo, C. Hydrogel Electrolytes Based on Xanthan Gum: Green Route towards Stable Dye-Sensitized Solar Cells. *Nanomaterials* **2020**, *10*, 1585. [[CrossRef](#)] [[PubMed](#)]
67. Weber, G.; Farris, F.J. Synthesis and Spectral Properties of a Hydrophobic Fluorescent Probe: 6-Propionyl-2-(Dimethylamino) Naphthalene. *Biochemistry* **1979**, *18*, 3075–3078. [[CrossRef](#)] [[PubMed](#)]
68. Gunther, G.; Malacrida, L.; Jameson, D.M.; Gratton, E.; Sánchez, S.A. LAURDAN since Weber: The Quest for Visualizing Membrane Heterogeneity. *Acc. Chem. Res.* **2021**, *54*, 976–987. [[CrossRef](#)] [[PubMed](#)]
69. Zeng, J.; Chong, P.L. Effect of Ethanol-Induced Lipid Interdigitation on the Membrane Solubility of Prodan, Acдан, and Laurdan. *Biophys. J.* **1995**, *68*, 567–573. [[CrossRef](#)]
70. Otaiza-González, S.; Cabadas, M.; Robert, G.; Stock, R.P.; Malacrida, L.; Lascano, R.; Bagatolli, L.A. The Innards of the Cell: Studies of Water Dipolar Relaxation Using the ACDAN Fluorescent Probe. *Methods Appl. Fluoresc.* **2022**, *10*, 044010. [[CrossRef](#)]
71. Thoke, H.S.; Tobiesen, A.; Brewer, J.; Hansen, P.L.; Stock, R.P.; Olsen, L.F.; Bagatolli, L.A. Tight Coupling of Metabolic Oscillations and Intracellular Water Dynamics in *Saccharomyces Cerevisiae*. *PLoS ONE* **2015**, *10*, e0117308. [[CrossRef](#)]
72. Vorontsova, I.; Vallmitjana, A.; Torrado, B.; Schilling, T.F.; Hall, J.E.; Gratton, E.; Malacrida, L. In Vivo Macromolecular Crowding Is Differentially Modulated by Aquaporin 0 in Zebrafish Lens: Insights from a Nanoenvironment Sensor and Spectral Imaging. *Sci. Adv.* **2022**, *8*, eabj4833. [[CrossRef](#)]
73. Begarani, F.; D’Autilia, F.; Signore, G.; Del Grosso, A.; Cecchini, M.; Gratton, E.; Beltram, F.; Cardarelli, F. Capturing Metabolism-Dependent Solvent Dynamics in the Lumen of a Trafficking Lysosome. *ACS Nano* **2019**, *13*, 1670–1682. [[CrossRef](#)]
74. Ambroggio, E.E.; Navarro, G.S.C.; Socas, L.B.P.; Bagatolli, L.A.; Gamarnik, A.V. Dengue and Zika Virus Capsid Proteins Bind to Membranes and Self-Assemble into Liquid Droplets with Nucleic Acids. *J. Biol. Chem.* **2021**, *297*, 101059. [[CrossRef](#)]
75. Mangiarotti, A.; Siri, M.; Tam, N.W.; Zhao, Z.; Malacrida, L.; Dimova, R. Biomolecular Condensates Modulate Membrane Lipid Packing and Hydration. *Nat. Commun.* **2023**, *14*, 6081. [[CrossRef](#)]
76. Parasassi, T.; De Stasio, G.; d’Ubaldo, A.; Gratton, E. Phase Fluctuation in Phospholipid Membranes Revealed by Laurdan Fluorescence. *Biophys. J.* **1990**, *57*, 1179–1186. [[CrossRef](#)] [[PubMed](#)]
77. Kim, M.; Im, S.; Park, I.; Kim, D.; Kim, E.S.; Joseph, J.; Yoon, J. Fabrication of Agar-Based Tissue-Mimicking Phantom for the Technical Evaluation of Biomedical Optical Imaging Systems. *Curr. Appl. Phys.* **2024**, *61*, 80–85. [[CrossRef](#)]
78. Jayawardena, I.; Turunen, P.; Garms, B.C.; Rowan, A.; Corrie, S.; Grøndahl, L. Evaluation of Techniques Used for Visualisation of Hydrogel Morphology and Determination of Pore Size Distributions. *Mater. Adv.* **2023**, *4*, 669–682. [[CrossRef](#)]
79. Lee, P.Y.; Costumbrado, J.; Hsu, C.Y.; Kim, Y.H. Agarose Gel Electrophoresis for the Separation of DNA Fragments. *J. Vis. Exp.* **2012**, *62*, 3923. [[CrossRef](#)]
80. Van Maarschalkerweerd, A.; Vetri, V.; Vestergaard, B. Cholesterol Facilitates Interactions between  $\alpha$ -Synuclein Oligomers and Charge-Neutral Membranes. *FEBS Lett.* **2015**, *589*, 2661–2667. [[CrossRef](#)]
81. Golfetto, O.; Hinde, E.; Gratton, E. Laurdan Fluorescence Lifetime Discriminates Cholesterol Content from Changes in Fluidity in Living Cell Membranes. *Biophys. J.* **2013**, *104*, 1238–1247. [[CrossRef](#)]
82. Soto-Arriaza, M.A.; Sotomayor, C.P.; Lissi, E.A. Relationship between Lipid Peroxidation and Rigidity in L- $\alpha$ -Phosphatidylcholine-DPPC Vesicles. *J. Colloid. Interface Sci.* **2008**, *323*, 70–74. [[CrossRef](#)]
83. Suhaj, A.; Le Marois, A.; Williamson, D.J.; Suhling, K.; Lorenz, C.D.; Owen, D.M. PRODAN Differentially Influences Its Local Environment. *Phys. Chem. Chem. Phys.* **2018**, *20*, 16060–16066. [[CrossRef](#)]
84. Krasnowska, E.K.; Bagatolli, L.A.; Gratton, E.; Parasassi, T. Surface Properties of Cholesterol-Containing Membranes Detected by Prodan Fluorescence. *Biochim. Biophys. Acta Biomembr.* **2001**, *1511*, 330–340. [[CrossRef](#)]
85. Chiu, Y.C.; Vo, T.H.; Sheng, Y.J.; Tsao, H.K. Spontaneous Formation of Microgels for a 3D Printing Supporting Medium. *ACS Appl. Polym. Mater.* **2023**, *5*, 764–774. [[CrossRef](#)]
86. Feiner, G. Additives: Phosphates, Salts (Sodium Chloride and Potassium Chloride, Citrate, Lactate) and Hydrocolloids. In *Meat Products Handbook*; Woodhead Publishing: Sawston, UK, 2006.
87. Leone, M.; Sciortino, F.; Migliore, M.; Fornili, S.L.; Vittorelli, M.B.P. Order Parameters of Gels and Gelation Kinetics of Aqueous Agarose Systems: Relation to the Spinodal Decomposition of the Sol. *Biopolymers* **1987**, *26*, 743–761. [[CrossRef](#)]
88. Gomes, C.; Dias, R.C.S.; Costa, M.R.P.F.N. Static Light Scattering Monitoring and Kinetic Modeling of Polyacrylamide Hydrogel Synthesis. *Processes* **2019**, *7*, 237. [[CrossRef](#)]
89. Munćan, J.; Mileusnić, I.; Šakota Rosić, J.; Vasić-Milovanović, A.; Matija, L. Water Properties of Soft Contact Lenses: A Comparative Near-Infrared Study of Two Hydrogel Materials. *Int. J. Polym. Sci.* **2016**, *2016*, 3737916. [[CrossRef](#)]

**Disclaimer/Publisher’s Note:** The statements, opinions and data contained in all publications are solely those of the individual author(s) and contributor(s) and not of MDPI and/or the editor(s). MDPI and/or the editor(s) disclaim responsibility for any injury to people or property resulting from any ideas, methods, instructions or products referred to in the content.